



## Continuous measurements of isotopic composition of water vapour on the East Antarctic Plateau

5 Mathieu Casado<sup>1,2</sup>, Amaelle Landais<sup>1</sup>, Valérie Masson-Delmotte<sup>1</sup>, Christophe Genthon<sup>4,5</sup>, Erik Kerstel<sup>2,3</sup>, Samir Kassi<sup>2</sup>, Laurent Arnaud<sup>4,5</sup>, Ghislain Picard<sup>4,5</sup>, Frederic Prie<sup>1</sup>, Olivier Cattani<sup>1</sup>, Hans-Christian Steen-Larsen<sup>6</sup>, Etienne Vignon<sup>4,5</sup>, Peter Cermak<sup>7</sup>

<sup>1</sup> Laboratoire des Sciences du Climat et de l'Environnement - IPSL, UMR 8212, CEA-CNRS-UVSQ, Gif sur Yvette, France

<sup>2</sup> CNRS, LIPHY, F-38000 Grenoble, France

10 <sup>3</sup> Univ. Grenoble Alpes, LIPHY, F-38000 Grenoble, France

<sup>4</sup> Univ. Grenoble Alpes, LGGE, F-38041 Grenoble, France

<sup>5</sup> CNRS, LGGE, F-38041 Grenoble, France

<sup>6</sup> Centre for Ice and Climate, University of Copenhagen, Denmark

15 <sup>7</sup> Department of Experimental Physics, Faculty of Mathematics, Physics and Informatics, Comenius University, Mlynska dolina F2, 842 48 Bratislava, Slovakia

*Correspondence to:* mathieu.casado@gmail.com

20 **Abstract.** Water stable isotopes in central Antarctic ice cores are critical to quantify past temperature changes. Accurate temperature reconstructions require to understand the processes controlling surface snow isotopic composition. Isotopic fractionation processes occurring in the atmosphere and controlling snowfall isotopic composition are well understood theoretically and implemented in atmospheric models. However, post-deposition processes are poorly documented and understood. To quantitatively interpret the isotopic composition of water archived in ice cores, it is thus essential to study the continuum between surface water vapour, precipitation, surface snow and buried snow.

25 Here, we target the isotopic composition of surface snow, precipitation and water vapour at Concordia Station, where the oldest EPICA Dome C ice cores have been retrieved. While snowfall and surface snow sampling is routinely performed, accurate measurements of surface water vapour are challenging in such cold and dry conditions. New developments in infrared spectroscopy enable now the measurement of isotopic composition in water vapour traces. Two infrared spectrometers have been deployed at Concordia, allowing  
30 continuous, in situ measurements for one month in December-January 2014-2015. Comparison of the results from infrared spectroscopy with laboratory measurements of discrete samples trapped using cryogenic sampling validates the relevance of the method to measure isotopic composition in dry conditions. We observe very large diurnal cycles in isotopic composition well correlated with temperature diurnal cycles. Identification of different behaviours of isotopic composition in the water vapour associated with turbulent or  
35 stratified regime indicates a strong impact of meteorological processes in local vapour/snow interaction. Even if the vapour isotopic composition seems to be, at least part of the time, at equilibrium with the local snow, the slope of  $\delta D$  against  $\delta^{18}O$  prevents us from identifying a unique origin leading to this isotopic composition.

40 **1. Introduction**

Ice cores from polar ice sheets provide exceptional archives of past variations in climate, aerosols, and global atmospheric composition. Amongst the various measurements performed in ice cores, the stable isotopic composition of water (e.g.  $\delta^{18}\text{O}$  or  $\delta\text{D}$ ) provides key insights in past polar climate and atmospheric water cycle. The atmospheric processes controlling this signal have been explored throughout the past decades using present day monitoring data. Based on the sampling of precipitation or surface snow, relationships between precipitation isotopic composition and local temperature have been identified since the 1960s, and understood theoretically to reflect atmospheric distillation processes (Dansgaard, 1964; Lorius et al., 1969). Nevertheless, there is both observational and modelling evidence that the isotope-temperature relationship is not stable in time and space (Jouzel et al., 1997; Masson-Delmotte et al., 2008). The variation in the isotope-temperature relationship have been explained by the isotopic composition of precipitation being sensitive to changes in condensation versus surface temperature, to changes in evaporation condition and transport paths, and to changes in precipitation intermittency (Charles et al., 1994; Fawcett et al., 1997; Krinner et al., 1997; LeGrande and Schmidt, 2006; Masson-Delmotte et al., 2011; Werner et al., 2011). While complex, these processes can be tracked using second order isotopic parameters such as d-excess, which preserve information on evaporation conditions (Jouzel et al., 2013; Landais et al., 2008) and they are accounted for by atmospheric models equipped with water stable isotopes (Risi et al., 2010; Schmidt et al., 2005; Werner et al., 2011).

The variations of d-excess and some variations in  $\delta^{18}\text{O}$  are due to the different influences of equilibrium fractionation and diffusion driven kinetic fractionation processes at each step of the water mass distillation trajectory. Specific limitations exist for the representation of the isotopic fractionation at very low temperature. Equilibrium fractionation coefficients have been either determined by spectroscopic calculations (Van Hook, 1968) or by laboratory experiments (Ellehöj et al., 2013; Majoube, 1971; Merlivat and Nief, 1967) with significant discrepancies at low temperatures. Molecular diffusivities have mainly been measured at 20°C (Cappa et al., 2003; Merlivat, 1978) but recent experiments have shown that temperature can have a strong impact on these coefficients (Luz et al., 2009).

Another source of uncertainty for the climatic interpretation of ice core records arises from poorly understood post-deposition processes. Indeed, the isotopic signal of initial local snowfall can be altered through wind transport and erosion, which are strongly dependent on local and regional topography, and can produce artificial variations in ice core water stable isotopes caused by gradual snow dune movement (Ekaykin et al., 2002; Ekaykin et al., 2004; Frezzotti et al., 2002). Moreover, it is well known that the initial isotopic signal associated with individual snowfall events is smoothed in firn, a process described as “diffusion” (Johnsen et al., 2000; Neumann and Waddington, 2004). This “diffusion” occurs through isotopic exchanges between surface water vapour and snow crystals during snow metamorphism (Waddington et al., 2002). “Diffusion lengths” have been identified based on spectral properties of ice core records and shown to depend on several processes: wind transport and erosion will alter the surface composition with a very strong influence of orography, diffusion through the pores of the snow firn smooths the signal as does metamorphism of the crystals (Schneebeli and Sokratov, 2004). Finally, there are hints based on high resolution isotopic measurements performed near snow surface for potential alteration of the initial precipitation isotopic composition (Hoshina et al., 2014; Sokratov and Golubev, 2009; Steen-Larsen et al., 2014a). This motivates investigations of the isotopic composition of precipitation, surface snow, but also of surface water vapour.

Atmospheric monitoring in extreme polar climatic conditions remains challenging. Supersaturation generates frost deposition which can bias temperature and humidity measurements, and low vapour contents are often outside of range of commercial instruments. As specific humidity is under 1000 ppmv on the central Antarctic plateau, measuring the isotopic composition of surface water vapour requires either very long cryogenic trapping (typically 10 hours at 20L/min) to collect enough material for off-line (mass spectrometric or laser-based) isotopic analyses, or very sensitive on-line (laser-based) instruments able to produce accurate in-situ isotopic measurements.



Recent developments in infrared spectroscopy now enable direct measurements of isotopic composition of the vapour in the field, without time-consuming vapour trapping. With careful calibration methodologies, these devices provide accuracies comparable with those of mass spectrometers (Bailey et al., 2015; Tremoy et al., 2011) and have already been used for surface studies in arctic regions (Bonne et al., 2015; Bonne et al., 2014; Steen-Larsen et al., 2014a).

The goal of our study is first to demonstrate the capability to reliably measure the isotopic composition of central Antarctic surface water vapour during summer, second to investigate the magnitude of its diurnal variations, in comparison with the corresponding results from central Greenland (Steen-Larsen et al., 2013), and third to highlight the impact of an intermittently turbulent boundary layer on the isotopic composition variations.

We focus on Concordia station, at the Dome C site, where the oldest Antarctic ice core record, spanning the last 800 000 years, has been obtained (EPICA, 2004). During the last 20 years, the French-Italian Concordia station has been progressively equipped with a variety of meteorological monitoring tools, documenting vertical and temporal variations in atmospheric water vapour (Ricaud et al., 2012). During summer, meteorological data depict large diurnal cycles in both surface air temperature and humidity (Genthon et al., 2013), which may result from either boundary layer dynamics and/or air-snow sublimation/condensation exchanges.

During the Antarctic summer of 2006-2007, cold trap samplings of water vapour were performed. Here, we report for the first time the results of this preliminary study together with continuous measurements performed during the austral summer of 2014-2015 using laser instruments with a specific methodology for low humidity calibration, as well as new cold trap sampling for laboratory measurements.

This manuscript is organised in two main sections to highlight the two different aspects of the study. First, section 2 describes the technical aspect: the site, the material deployed and the applied methods, with a focus on calibration in order to assess the technical reliability of such methods for sites as cold as the Antarctic Plateau. Section 3 reports the scientific aspect of the results, with first a focus on the relevance of infrared spectroscopy compared to cryogenic trapping, second a description of the diurnal to intra-seasonal surface vapour isotopic variations and third an analysis of the origin of the vapour. We conclude and discuss outlooks for this work in Section 4.

## 2. Technical challenges

### 2.1. Sampling site

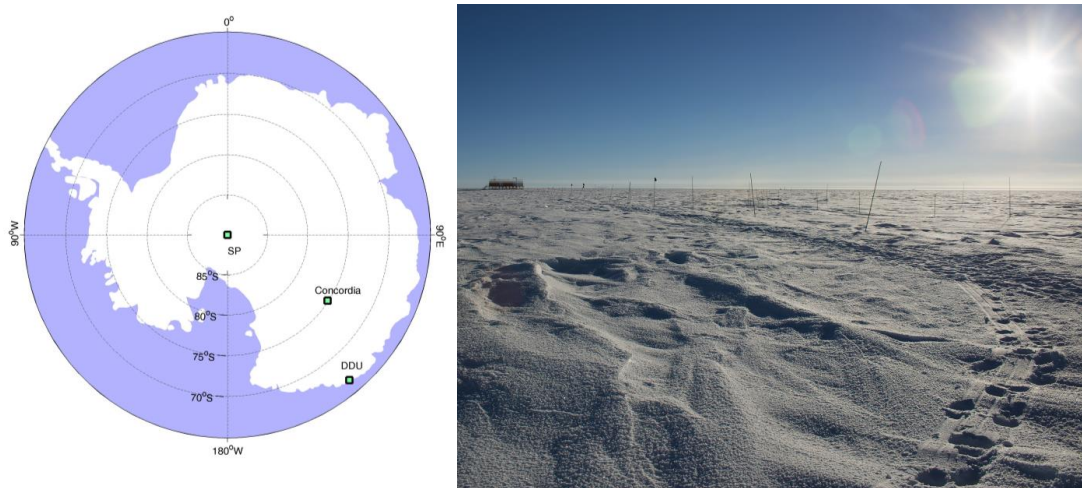
Concordia station is located near the top of Dome C at 75°06'06"S - 123°23'43"E, 3233 m above sea level and 950 km from the coast. While the local mean temperature is -54.3°C, it was -32.4°C during the campaign of 2014/2015 reaching a maximum value of -24.5°C. Ice core data suggest an average annual accumulation of  $2.7 \pm 0.7 \text{ g.cm}^{-2}.\text{yr}^{-1}$  (Genthon et al., 2015; Petit et al., 1982; Röthlisberger et al., 2000).

The first cold trap vapour sampling campaign was performed in summer 2006-2007. The second field campaign took place from December the 24<sup>th</sup> 2014 to January the 17<sup>th</sup> 2015.

The spectrometers for the 2014/2015 campaign were installed in an underground shelter located 800m upwind from the station, therefore protected from the fumes of the power generator of the station (discussed in section 2.5). Such underground shelter allows us to avoid any impact of the monitoring structure on the wind field and possible sampling artefacts. The area around the shelter is characterized by few sastrugi, none



135 higher than 20cm (Figure 1). A clean area of 12m<sup>2</sup> with no sastrugi was marked around the inlets. We decided to point the inlets toward the dominant wind in order to prevent artefacts from condensation or evaporation from the protection of the inlet or the pole holding it. Indeed, frost formation was observed on the protective foam and pole.



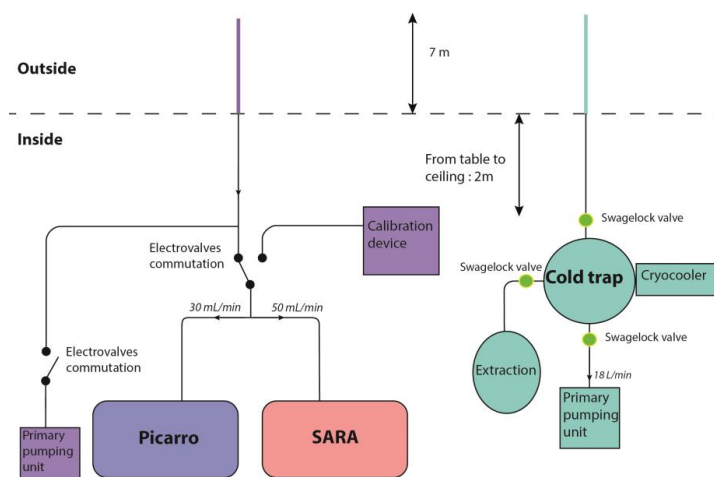
140 *Figure 1: Map of Antarctica showing the location of Concordia, Dumont d'Urville station (DDU) and the South Pole (SP). Picture of the area from the top of the underground shelter where the instrument was located looking toward the clean area.*

145 Together with our water vapour isotopic data, we use meteorological observations from the lowest level of the 45m meteorological profiling system at Dome C (Genthon et al., 2013). The profiling system was located at proximity with the spectrometers. The temperature observations on the 45m profiling system are made in aspirated shields and thus not affected by radiation biases. Genthon et al. (2011) demonstrated that when the wind speed is below 5m.s<sup>-1</sup>, radiation biases are very significant and can reach more than 10°C in conventional (non-wind ventilated) shields. Temperature is measured using HMP155 thermohygrometers, wind speed and direction using Young 05103 and 05106 anemometers. Elevation above the snow surface was 3.10m for the wind and 2.58m for temperature in 2014-15. This will be henceforth commonly referred as the 3m level. Further details on the observing system, instruments, sampling and results are available in previous publications (Genthon et al., 2013; Genthon et al., 2010). Surface temperature is measured with a Campbell scientific IR120 infrared probe. The probe is located at 2 meters height and uses upwelling infrared radiation and the temperature of the detector to compute the temperature of the surface of the snow. The uncertainty of the surface temperature measurement is around ±1°C which is mainly due to unknown and possibly varying emissivity of the snow (Salisbury et al., 1994).

160

## 2.2. Water vapour isotope monitoring

165 Two infrared spectrometers were used to measure continuously the isotopic composition of water vapour pumped 2 meters above the snow surface: a Cavity Ring-Down Spectrometer (CRDS) from Picarro (L2130-i) and a High-Finesse water Isotope spectrometer (HiFi) based on the technique of optical feedback cavity enhanced absorption spectroscopy (OFCEAS) developed in LIPhy, Grenoble, France (Landsberg et al., 2014) as described on figure 2.



170

*Figure 2: Schematics of the experimental set up implied in the water vapour isotopic composition monitoring*

Both instruments are based on a general technique of cavity enhanced absorption spectroscopy (Romanini et al., 2014). This is essentially a long path length optical detection technique that increases the sensitivity of detection of molecules in the optical cavity by folding the optical beam path between two (or three) highly reflective mirrors. The commercial Picarro spectrometer is based on near-infrared continuous-wave cavity ring-down spectroscopy (CW-CRDS) (Crosson, 2008). It has proven to be a fairly robust and reliable system, delivering good precision isotopic measurements at concentration (water mixing ratio) values between 1000 and 25000 ppmv.

175

180

The HiFI spectrometer is also operating in the near-infrared region of the spectrum, but uses another implementation of cavity enhanced absorption spectroscopy called optical feedback cavity enhanced absorption spectroscopy (OFCEAS) (Romanini et al., 2014). In the case of the HiFI spectrometer, the optical path length was increased by about one order of magnitude to 45 km. This optimizes the spectrometer for oxygen-18 isotopic measurements with a precision better than 0.05‰ at a water mixing ratio around 500 ppmv (Landsberg et al., 2014). The HiFI spectrometer was shown to be able to reach this level of performance also in Antarctica during a 3-week campaign at the Norwegian station of Troll (Landsberg, 2014). Unfortunately, during the current campaign at Dome C, the spectrometer had to operate in a noisy environment. The system was not isolated from vibrations of several vacuum pumps in the shelter and an accidental resonance did perturb the phase control. This resulted in a baseline noise level more than one order higher than normal, which created a corresponding increase of the error on the isotope ratio measurements. At this level of noise, the Picarro measurements turned out to be more precise than the HiFI measurements. It is for this reason that the latter were only used as an independent tool to check on the absolute values from Picarro measurements. All time-series shown hereafter were obtained with the Picarro spectrometer.

185

190

195

The two instruments were connected through a common heated inlet consisting of a ¼ inch copper tube. The internal pumps of each instrument pumped the outside vapour through the common inlet and into the respective cavities. The fluxes generated by the instruments were small enough not to interact with one another, as attested by stable pressure in the cavities of both instruments. The length of this common inlet (approximately 10m long) caused a response delay of approximately 2 minutes for the humidity signal. Memory effects caused by interactions between the water vapour and the inside of the tubes introduce different delays for different isotopes. As a result for high resolution data, artificial d-excess can be produced as the memory effect of HDO is substantial larger than H<sub>2</sub><sup>18</sup>O (Steen-Larsen et al., 2014b). However our

200



205 measurements were averaged over 1 hour thereby removing this effect. No sign of condensation in the inlet  
was observed during the whole campaign.

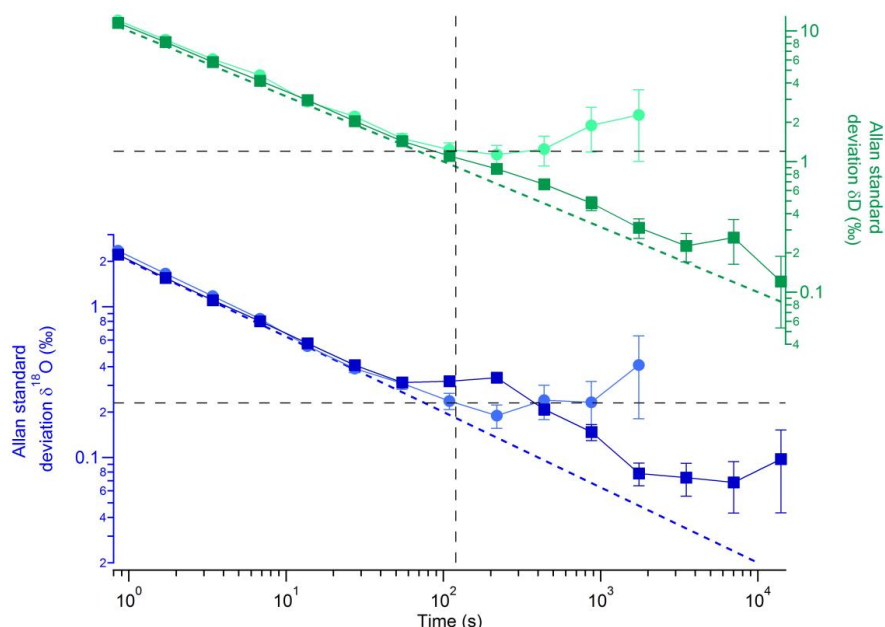
### 2.3. Allan variance analyses

210 The measurements of isotopic composition with an acquisition time of approximately 1 second have a  
standard deviation of 10‰ for  $\delta\text{D}$  and of 2‰ for  $\delta^{18}\text{O}$  at approximately 500 ppmv (Figure 3). Infrared  
spectrometers typically produce data perturbed by different kinds of noise: one is noise due to frequency  
instabilities of the laser, temperature and mechanical instabilities of the cavity, temperature and pressure of  
the sampled gas, electronic noise, and residual optical interference fringes on the spectrum baseline. This  
noise, usually predominantly white noise, can be significantly reduced through time averaging: for instance,  
215 with an acquisition time of 2 minutes, we decrease the standard deviation to 1.3‰ for  $\delta\text{D}$  and 0.2‰ for  $\delta^{18}\text{O}$ .

With increasing integration time, one expects the precision of the measurements to initially improve, due to  
the reduction of white noise, up to the point where instrumental drift becomes visible. The so-called Allan-  
Werle plot shows the overall expected precision as a function of integration time (Figure 3).

220 Laboratory long term measurement of a standard was realised at a humidity of  $506 \pm 3$  ppmv in order to  
reproduce the range of the expected humidity for Concordia station. Stable humidity production for 13 hours  
was realised using the calibration device described in the next section. The standard deviation of  $\delta\text{D}$  follows  
the optimum line almost up to 4 hours integration time. The standard deviation of  $\delta^{18}\text{O}$  does not follow the  
optimum profile after 100 seconds but still drops continuously over almost 2 hours. These measurements  
225 confirm the reliability of the Picarro L2130i even at low humidity and justify the use of such an instrument in  
this campaign. The integration time providing the ultimate precision could not be achieved because of the  
lack a vapour generator stable for more than 13 hours. At other humidity levels, we observe similar profile  
with an increasing initial precision as the moisture content increases (not shown).

230 In the field, we performed calibrations lasting up to 90 minutes, as a trade-off between instrument  
characterization and measurement time optimization. This, however, is not long enough to accurately  
estimate the rise of uncertainty due to instrumental drift, but allows us to assess the ultimate precision for the  
instruments under realistic field conditions. The Allan variance was thus calculated from field Picarro  
235 calibration data, at 450 ppmv. From this analysis, we conclude that 2 minutes appear to provide an optimal  
integration time, associated with an ultimate precision of the spectrometer of 0.2‰ for  $\delta^{18}\text{O}$  and 1.1‰ for  $\delta\text{D}$   
(black dashed lines on figure 3). This test could not be performed at other humidities.



240 *Figure 3: Allan variance plots for laboratory long term standard measurement (dark squares) and for field*  
*long term standard measurement (light circles) for  $\delta D$  (Top, green) and for  $\delta^{18}O$  (bottom, blue). Dash lines*  
*correspond to the quantum limit on  $N^{-1/2}$  for each composition.*

## 2.4. Calibrations

245

Calibration of the spectrometer is crucial in order to be able to express the measurement results with confidence on the international VSMOW2-SLAP2 isotope scale (IAEA, 2009). Calibrations have been reported to vary between instruments and calibration systems, as well as over time. Tremoy et al. (2011) highlighted the importance of calibration for Picarro analysers under 10 000 ppmv with biases up to 10‰ for  $\delta D$  and of 1‰ for  $\delta^{18}O$  at volume mixing ratios (VMR) down to 2000 ppmv. Protocols have been developed and adapted for calibration under Greenland ice sheet summer (Steen-Larsen et al., 2013) and south Greenland year-round conditions (Bonne et al., 2014) with good performance attested from parallel measurements of PICARRO and LGR analysers for humidity above 2000 ppmv. At VMRs below 2000 ppmv, much larger errors can be expected without calibrating the instruments. For this field season, we have followed the team classical calibration protocols with (1) a study of the drift of the instrument, (2) a linearity calibration using two working standards whose isotopic values were established in the laboratory versus SMOW and SLAP and (3) a study of the influence of humidity on the isotopic value of the water vapour. Because we are working at very low humidity, we could not use standard water vapour generator and had to develop our own device.

260

Standard calibration devices cannot be used to produce humidity levels as low as the one encountered on the Antarctic Plateau (under 1000 ppmv). We therefore built our own calibration device in order to produce vapour with known isotopic composition at low concentration. This home-made calibration device is inspired from the device developed by Landsberg (2014). It consists of an infuse/withdraw pump 11 elite from Harvard Apparatus, which can produce a water flow as low as 3.66pl/min with an accuracy is of the order of 0.5%. This pump pushes water through a needle toward an evaporation chamber with a controlled dry air laminar flow. The airflow can be controlled between 0 and 500 standard cubic centimetre per minute (scm)

265



with a precision of 4 sccm over a pressure range from 100 to 1000 hPa by Bronkhorst devices. The main improvement for this version of the calibration device is the integration of a 3 ways liquid valve which enables one to switch between a withdraw and an infuse mode to either pump water from a reservoir or push it toward the needle. Apart from the obvious convenience brought by this addition, the valve is connecting the syringe, the water reservoir and the needle with air tight connexions increasing the robustness and successfully eliminating the presence of air bubbles in the water sampled by the syringe.

When a water drop forms at the tip of the needle, the diameter of the drop is transiently adjusted up to the point when the inflow of liquid water in the needle is compensated by evaporation: at this stage, the drop remains at the tip of the needle and a constant flow of vapour is produced. When the permanent regime is reached (within a few minutes), the isotopic composition of the evaporated vapour is exactly the isotopic composition of the water injected, and the humidity level is completely controlled by the inflows of liquid water and air, therefore independent of local thermodynamic properties such as temperature or pressure. By propagating the uncertainty for the air fluxes (1%) and water flux (0.5%) to the conversion formula to calculate the humidity, we estimate the uncertainty associated with this humidity production of the order of 2%. Experimentally, standard deviation on the specific humidity measured during the different sets of calibration is usually between 1 and 5 ppmv. This leads to an uncertainty of 1 to 2% of the specific humidity. The production of humidity by the calibration device is therefore more precise than the measurements of the Picarro and HIFI.

The 3 types of calibrations were performed in the field and in the laboratory prior and after field work. It was particularly important to add laboratory calibrations (especially for drift of the instrument) in addition to field calibrations because of the short season and lack of dry air at the beginning of the season, in particular to strengthen the results from type (2) and (3) calibrations.

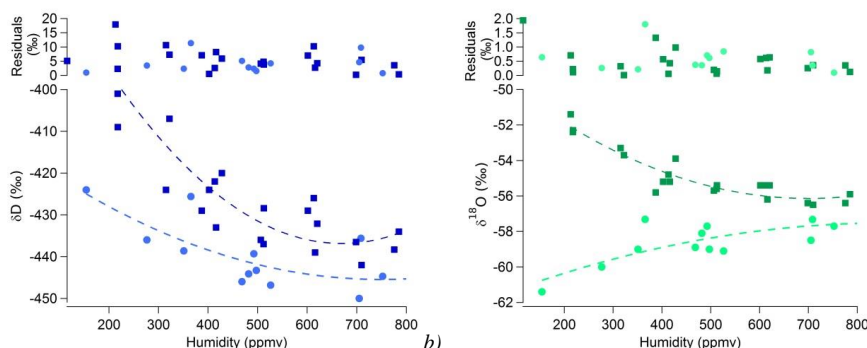


Figure 4: Measured isotopic composition for a)  $\delta D$  and b)  $\delta^{18}O$  using the PICARRO spectrometer for a fixed humidity: light circles are field calibration points, dark squares are laboratory calibration points, the dashed lines are the fit with a quadratic function and on top are the residuals compared to the fit for the entire series.

In order to estimate the drift of our infrared spectrometers, a series of calibration was performed in the laboratory from 100 to 1000 ppmv and repeated on five occasions in a time span of 4 weeks. Later on in this manuscript, we refer to a calibration as a measurement of one standard at one known humidity lasting around 30 minutes, as soon as the generated vapour reaches the stability threshold of 2% on the humidity. The measured value of the isotopic composition averaged over these 30 minutes is then compared to the average value of humidity. Each set of calibrations, provided that it was achieved within the same day, can be fitted by a quadratic function with a small dispersion of the data points (inferior to 2% for  $\delta D$  and 0.2 % for  $\delta^{18}O$ ). Different calibration sets performed over different days show dispersion due to the instrument drift. We observe a much larger dispersion for  $\delta D$  than for  $\delta^{18}O$ , at low concentration (200 ppmv) (see table 1.). Note that the low residuals for the field calibration at 150 ppmv are an artefact due to few measurements at this humidity.



310 *Table 1: Average residuals compared to the quadratic fit toward humidity of laboratory (5 sets) and field*  
315 *calibrations for different humidity levels for the Picarro, cf figure 4a) and b).*

Laboratory calibrations	Humidity (ppmv)	200	400	600	800
	$\delta\text{D}$ residuals (‰)	10.1	4.9	6.0	3.1
	$\delta^{18}\text{O}$ residuals (‰)	0.3	0.7	0.5	0.3
Field calibrations	Humidity (ppmv)	150	350	480	710
	$\delta\text{D}$ residuals (‰)	1.0	6.8	2.9	5.1
	$\delta^{18}\text{O}$ residuals (‰)	0.6	1.0	0.5	0.4

320 Field calibration could only be performed after the 7<sup>th</sup> of January when the dry air bottle was delivered to  
Concordia. Then, 2 calibrations per day were realised as follow: 30 minutes calibration, 30 minutes  
325 measurements of outside air and 30 minutes calibration. As the data are interpolated on an hourly resolution,  
this procedure prevents gaps in the data. Altogether, 20 calibrations were achieved from January 7<sup>th</sup> to  
January 17<sup>th</sup> with two working standards. As it was not possible to perform relevant ramps of humidity within  
one day, all the calibrations were merged into one series (Figure 4, light colour points). This merged field  
330 calibration set provides with an estimate of the linear correction to be applied on the measured humidity (cf  
supplementary material part 1). The merged field calibration series also documents the non-linearity of the  
instrument as a function of the background humidity level and is used to correct the values of  $\delta\text{D}$  and  $\delta^{18}\text{O}$   
measurements in water vapour. The laboratory and field calibrations do not match, which is not unexpected.  
335 Calibrations realised in the lab and in the field have been reported to differ (Aemisegger et al., 2012) which  
rules out the use of pre-campaign laboratory calibrations, even though laboratory calibration is still useful to  
provide insight in the minimum error to be expected during the field campaign. For both laboratory and field  
calibrations, large residuals are observed for  $\delta\text{D}$  at low humidity (200 ppmv). Based on the mean residuals  
compared to the fits, we estimate the accuracy of our measurements to be 6‰ for  $\delta\text{D}$  and 0.7‰ for  $\delta^{18}\text{O}$ .

We cannot estimate from these measurements the drift over the period of field measurement. However, we  
incorporate an uncertainty for this drift from the laboratory calibrations. These laboratory calibrations were  
340 realised on a period longer than the campaign and therefore should bracket the actual drift of our instrument  
during field deployment. The impact of the drift over several weeks on the laboratory calibrations is visible  
on figure 4 by the spread of the different calibration sets.

The uncertainty on the absolute value is calculated from the largest residuals of both the laboratory and field  
345 calibration fit. It rises up to 18‰ for  $\delta\text{D}$  at 200ppmv and 1.7‰ for  $\delta^{18}\text{O}$  at 400ppmv, with better accuracy at  
higher humidity (Figure 4). This highlights the need for regular calibrations to obtain the best performances.  
For this study, the lack of regular calibrations hinders by a factor of 5 the precision of the measurements  
(1.3‰ for  $\delta\text{D}$  in the best conditions from the Allan Variance against 6‰ for  $\delta\text{D}$  from the mean residuals of  
350 the calibration). Additional information about the linearity of Picarro infrared spectrometers against the  
SMOW-SLAP scales at isotopic composition below the SLAP values can be found in section 2.6 with the  
description of the measurements of the cryogenic trapping samples.

## 2.5. Data post-treatment and performances

355 In addition to the calibration and averaging necessary to improve the accuracy and precision of the dataset,  
we had to correct our data from the introduction of condensate inside the inlet. Figure 5 illustrates two of  
such “snow-intake” events, providing typical examples of duration and shape. Indeed, our inlet was facing  
the dominant wind without any protection to prevent introduction of condensates. Such protection usually

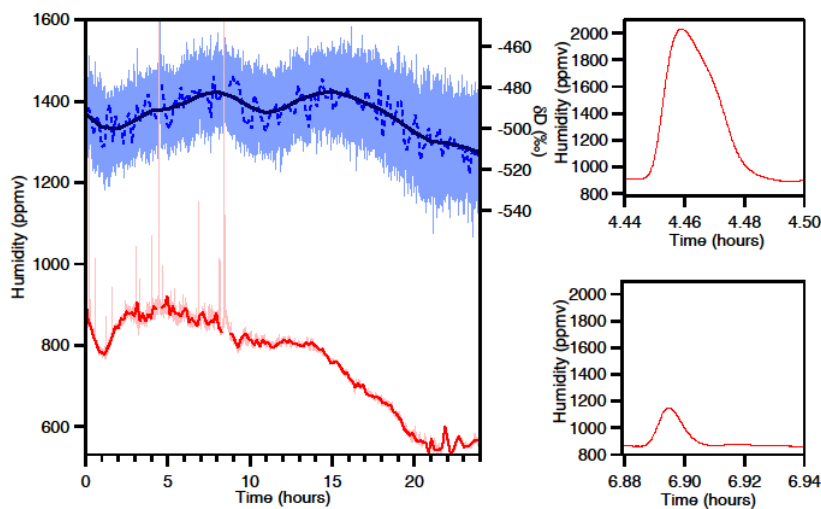


360 requires to be heated to prevent condensation of water vapour under supersaturated conditions; however  
heating would lead to sublimation of all the precipitation falling into the inlet, which would then increase the  
vapour content. Moreover, micro droplets or crystals are often floating in the air on the Antarctic Plateau, and  
reduce the efficiency of any precipitation filter. We therefore decided to remove the effect of all sort of  
precipitation events through a post-treatment of our datasets. This is justified by a small number of cases  
(fewer than 100), clearly identified as “snow-intake” events.

365 A manual post-treatment was thus realised following systematic rules. All data with a specific humidity  
higher than 1000ppmv were discarded: this value was chosen as the maximum surface air temperature  
observed during the campaign ( $-24.6^{\circ}\text{C}$ ) implies a theoretical maximum saturated vapour content of 1030  
ppmv. After this first post treatment, the largest humidity measurements of 977 ppmv, slightly lower than the  
maximum saturated vapour content suggesting that we may have discarded only a few relevant high humidity  
data in our post-processing.

370 All humidity peaks higher than natural variability were also discarded, using as a threshold 5 times the  
standard deviation in normal conditions (which is between 10 and 20ppmv). In very few occasions (only 2  
during the entire campaign), a very high density of snowflakes could create a regular inflow of snow in the  
inlet, leading to an increase of the vapour content without peak shapes. In those cases, the amplitude and the  
frequency of the specific humidity variability still allowed us to distinguish precipitation introduction from  
375 the “background” vapour signal. These periods associated with important “snow-intakes” created gaps in the  
dataset (4 hours in total). Gaps in our dataset mostly arise from calibration of the instruments and power  
shortages (30 to 60 minutes gaps) that could be filled by interpolating.

Two running averages were performed: first at 10 minutes resolution, without filling the gaps which  
corresponds to approximately 3% of the dataset (figure 5), then an average at a resolution of the hour where  
380 the gaps were filled by linear interpolation (only 1% of the whole datasets had gaps superior than an hour)  
apart from the 13<sup>th</sup> of January when 4 hours in a row were missing due to intense precipitation event. Finally,  
0.7% of the dataset is missing at the 1 hour resolution.



385 *Figure 5:* left : example of raw data measured by the Picarro: humidity (light red, ppmv) and  $\delta D$  (light blue, ‰), data averaged over 10 minutes for humidity (red, ppmv) and for  $\delta D$  (dashed line blue, ‰) and over 1 hour for  $\delta D$  (dark blue, ‰). Right: zoom on two “precipitation events” identified in the humidity signal of the Picarro (top, snow flake; bottom, diamond dust).



390 Even though the spectrometer was located at the border of the clean area of the station, we verified that the  
influence of the station did not contaminate the vapour by analysing wind direction. As mentioned earlier, the  
shelter is almost 1km upstream the station against the dominant wind. Few events with wind direction  
pointing from the station were identified (21 hours spread over 5 days during the whole campaign where the  
wind direction is pointing from the station plus or minus 20°). Most of these events match the period when  
the wind speed was very low ( $< 2 \text{ m.s}^{-1}$ ). We used the methane measurements also provided by the Picarro  
L2130 in parallel with the vapour measurements to assess any potential anthropic contamination of the  
395 vapour at the shelter area. An anthropic contamination of the vapour could lead to artificial values of isotopic  
composition. Indeed, combustion of fossil fuels have been shown to produce d-excess for instance (Gorski et  
al., 2015). Small spikes of methane were detected for only two occurrences: December the 28<sup>th</sup> between 9:30  
and 10:40 and January the 3<sup>rd</sup> between 6:00 and 7:00 (local time). They match events with wind direction  
pointing at the shelter. These two events were fairly short and no specific impact on either humidity or  
400 isotopic composition can be identified for these events.

## 2.6. Cryogenic trapping of the moisture

405 Water vapour was trapped with a cryogenic trapping device (Craig, 1965) consisting of a glass trap immersed  
in cryogenic ethanol. Cryogenic trapping has been proven reliable to trap all the moisture contained in the air  
and therefore to store ice samples with the same isotopic composition as the initial vapour (Helliker et al.,  
2002; Steen-Larsen et al., 2011). During the 2006/2007 campaign, 20 samples were gathered by cold traps  
immersed in ethanol at  $-77^\circ\text{C}$ , with a pump with a flow of 6L/min and 36hour sampling periods. For the  
campaign of 2014/2015, 20 samples were gathered by cold traps filled with glass balls immersed in ethanol  
410 at  $-100^\circ\text{C}$  under a flow of 18L/min and 10 to 14 hours trapping periods. The samples were extracted from the  
traps by heating them up to  $200^\circ\text{C}$  on a line under vacuum connected to a glass phial immersed in the  
cryogenic ethanol. This process allows the total transfer of the water by forced diffusion and produces  
samples between 2 to 4 mL. On January the 8<sup>th</sup> 2015, the high flux pump was damaged and was replaced by a  
membrane vacuum pump with only 8L/min flow increasing the trapping duration to 24 to 36 hours.

415 As no particles filter was installed on the inlet (cf section 2.1.), we trapped both the precipitation captured by  
the inlet and the surface vapour. This might lead to biases when precipitation occurred, and must be taken  
into account when comparing the results between the spectrometers and the cold trap.

420 Samples from the 2014/2015 campaign were then shipped for laboratory analyses using a Picarro L2140i.  
The samples were injected through a syringe in a vaporiser and an auto-sampler. The classical calibration  
procedure to analyse polar samples is using three internal standards calibrated against SMOW and SLAP  
(Standard Mean Ocean Water and Standard Low Antarctic Precipitation): NEEM ( $\delta^{18}\text{O} = -33.56\text{‰}$  and  $\delta\text{D} =$   
 $-257.6\text{‰}$ ), ROSS ( $\delta^{18}\text{O} = -18.75\text{‰}$  and  $\delta\text{D} = -144.6\text{‰}$ ) and OC3 ( $\delta^{18}\text{O} = -54.05\text{‰}$  and  $\delta\text{D} = -424.1\text{‰}$ ). The  
425 isotopic composition of the sample to analyse has to be surrounded by the isotopic composition of the  
standards for the calibration to be efficient. As the isotopic composition of the vapour in Concordia is well  
below SLAP ( $\delta^{18}\text{O} = -55.50\text{‰}$  and  $\delta\text{D} = -427.5\text{‰}$ ), i.e.  $\delta^{18}\text{O}$  is around  $-70\text{‰}$ , no standard was available to  
bracket the sample isotopic composition. It was therefore important to check the linearity of the instruments  
for  $\delta^{18}\text{O}$  values below  $-55\text{‰}$ .

430 In order to do so, we prepared new home made standards: we diluted a known home-made standard EPB  
( $\delta^{18}\text{O} = -7.54 \pm 0.05\text{‰}$ ) with highly depleted water Isotec Water- $^{16}\text{O}$  from Sigma-Aldrich (99.99% of  $^{16}\text{O}$   
atoms, here after DW for depleted water). We first had to determine the absolute composition of the depleted  
water by realising several dilutions of the water with isotopic composition in the range between SMOW and  
435 SLAP. The dilution was realised with a Sartorius ME215P scale, whose internal precision is certified at  
0.02mg. The water was injected through needles in a glass bottles covered by paraffin films to prevent  
evaporation. All the weights were measured 4 times in order to improve the precision of the measurements.



440 From the different measurements, the accuracy is estimated at 0.1 mg after correcting for the weight of the air removed from the bottle by injecting the water. Four new home-made standards were realised in the range SMOW/SLAP and measured 15 times each with a Picarro L2140i (cf figure 6, part 1). Their isotopic composition is scattered along the line from the EPB composition to the depleted water composition. Because we know the exact dilution of EPB with the depleted water, we can use the measured  $\delta^{18}\text{O}$  values to precisely infer the isotopic composition of the depleted water  $\delta^{18}O_{DW}$  or  $R_{DW}^{18} = (\delta^{18}O_{DW}/1000 + 1) * R_{SMOW}^{18}$  where  $R_{SMOW}^{18} = 2005.2$  is the absolute isotopic composition of the SMOW in  $\text{H}_2^{18}\text{O}$ .

445

The isotopic composition of the mix is given by:

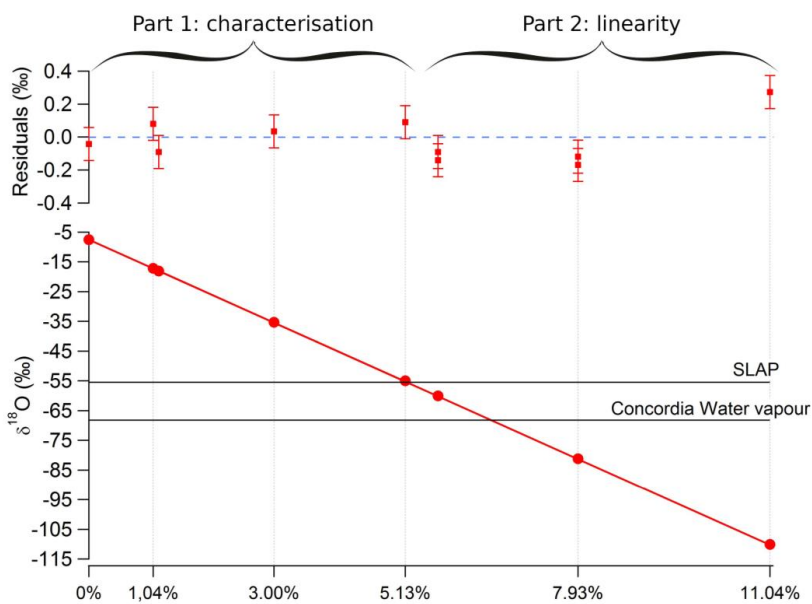
$$\delta^{18}O_{mix} = \delta^{18}O_{EPB} + \frac{R_{DW}^{18} - R_{EPB}^{18}}{R_{SMOW}^{18}} X_{DW} \quad (1)$$

450 where  $X_{DW}$  is the ratio of quantities of depleted water vs EPB in the dilution. The slope of the linear regression of  $\delta^{18}O_{mix}$  with  $X_{DW}$  provides directly an estimate of the isotopic composition of the depleted water. We find  $R_{DW}^{18} = 128 \pm 2$  (equivalent to  $\delta^{18}O_{DW} = -936.2 \pm 0.6 \text{‰}$ ), hence slightly less depleted than the specifications given by the producer (purity of 99.99%). Another determination can be done independently by using the formula (1) for one single dilution. Using independent dilutions done within the range SMOW/SLAP, we obtain  $R_{DW}^{18} = 127$  and 130.

455 In a second step, we produce 3 other water homemade standards by dilution of EPB with “almost pure”  $\text{H}_2^{16}\text{O}$  to obtain  $\delta^{18}\text{O}$  values below SLAP. Using the know dilution amount and the isotopic ratio of “almost pure”  $\text{H}_2^{16}\text{O}$  determined above, we compare the measurements for these 3 homemade standards, i.e. placed on a SMOW-SLAP scale with classical calibration procedure to the values calculated using formula (1) (figure 6, part 2.). Given the precision on the isotopic ratio of the “almost pure”  $\text{H}_2^{16}\text{O}$ , on the EPB and the precision of the scale, the precision of the calculation of  $\delta^{18}O_{mix}$  is 0.05‰ (uncertainty propagation in formula (1)).

460

465 Residuals between measured and calculated  $\delta^{18}\text{O}$  are less than 0.2‰ for the homemade standards at -60‰ and -80‰ and less than 0.3‰ at -110‰. We thus conclude that the Picarro L2140i can be used safely to infer linearly  $\delta^{18}\text{O}$  values down to -80‰ which encompasses the  $\delta^{18}\text{O}$  range of our water vapour samples; and is close to be linear for  $\delta^{18}\text{O}$  values down to -110‰ (deviation of 0.3‰ slightly higher than the measurement uncertainty).



470 *Figure 6:* Isotopic composition measured by liquid injector in the Picarro L2140i for different samples  
prepared by dilution of EPB with “almost pure” water, the red dots are the measurements, the red line is the  
calculated isotopic composition and the red squares for residuals are the difference between the  
measurements and the theoretical composition.

### 3. Results

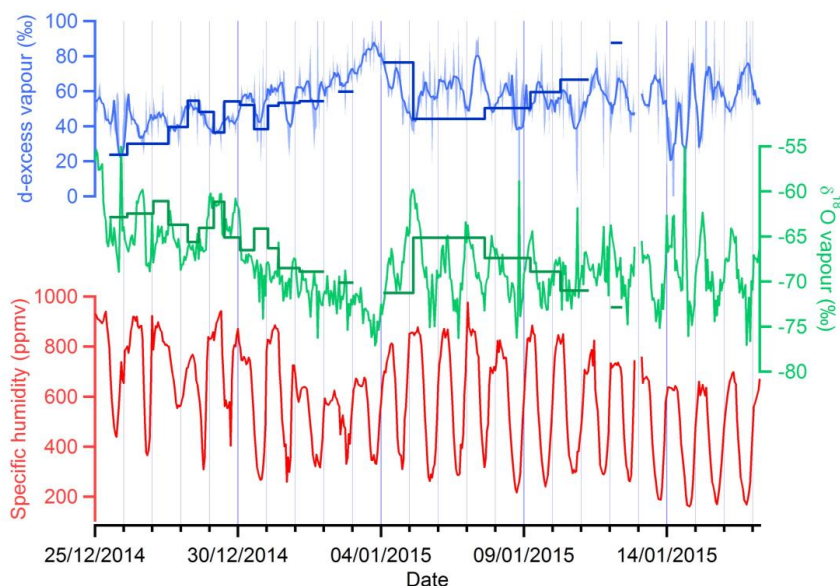
475

#### 3.1. Validation of infrared spectrometry data

480 The data gathered by the cold trap and the infrared spectrometers during the 2014/2015 campaign are  
displayed in Figure 7.

480

485 The measurements performed by the Picarro (light lines) from December the 25<sup>th</sup> to January the 4<sup>th</sup> are  
marked by a 10‰ gradual decline in  $\delta^{18}\text{O}$ , and a 40‰ gradual increase in d-excess. By contrast, the second  
part of the measurements (performed after January, the 4<sup>th</sup>) does not show any long term multi-day trend. We  
also observe a decrease in  $\delta^{18}\text{O}$  and an increase in d-excess in the cold trap data from December 25<sup>th</sup> to  
January 5<sup>th</sup>. These decrease in  $\delta^{18}\text{O}$  and increase in d-excess are also recorded in the period from the 5<sup>th</sup> of  
January to the 13<sup>th</sup> of January in the cold trap results while they are not observed in the Picarro data.



490 *Figure 7: hourly average  $\delta^{18}\text{O}$  (‰) in green, raw d-excess (‰) in light blue (d-excess smoothed on a 3 hours span in thick blue), and hourly average of the specific humidity (ppmv) in red during the campaign 2014/2015. Measurements by the Picarro are displayed as the thin light lines and measurements performed in the laboratory from the cold trap samples are displayed as dark bars.*

495 During a similar campaign from Greenland (Steen-Larsen et al., 2011), differences between infrared spectrometry in situ and cryogenic trapping measurements were generally around 0.1 ‰ in  $\delta^{18}\text{O}$ . In comparison, we observe that the cold trap  $\delta^{18}\text{O}$  values are generally higher than the  $\delta^{18}\text{O}$  measured by the Picarro. This can be explained by several factors. First, the isotopic composition sampled using the cold trap is weighted by humidity: the cold trap is trapping more moisture when the humidity is highest, which also corresponds to the moment when the isotopic composition is the highest. In order to take this into account, we weighted the isotopic composition from the Picarro by specific humidity (not shown). In average, the weighted isotopic composition has an offset of +1.1‰ in  $\delta^{18}\text{O}$  compared with the original dataset, rising up to 7.2‰ on December the 31<sup>st</sup> and down to -2.9‰ on January the 6<sup>th</sup>. In this case, the cold trap  $\delta^{18}\text{O}$  is still in average higher than the isotopic composition weighted by humidity, with an offset of +1.16‰ for  $\delta^{18}\text{O}$  and -3‰ for d-excess, which lies within the error bar of our measurements. We thus conclude that, at first order, our cold trap measurements validate the laser spectrometer data.

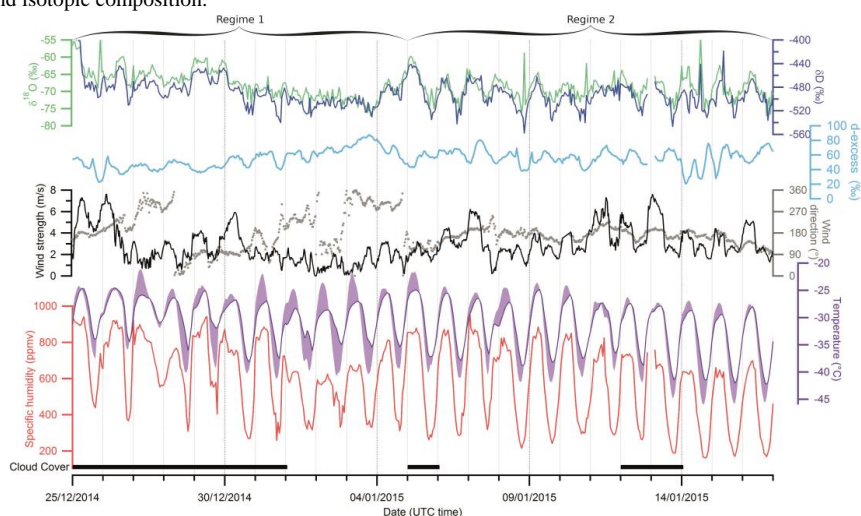
510 The cold trap measurements may also include snow-intake events that were captured by the inlet, whereas we removed such data in the spectrometer measurements. Because the isotopic composition of precipitation is enriched compared to the vapour, the introduction of snow crystals in the cold trap inlet could explain a small part of the positive offset of cold trap measurements compared to the infrared spectrometry. No quantitative estimation of this bias has been realised.

### 3.2. Two climatic regimes

515 Figure 8 presents the specific humidity and isotopic composition ( $\delta^{18}\text{O}$ ,  $\delta\text{D}$  and d-excess) measured by the Picarro. The data are continuous from December 25<sup>th</sup> 2014 to January 17<sup>th</sup> 2015, except for 4 hours on



January 13<sup>th</sup> due to a large snowfall event. These data are compared with the 3m temperature and the 3m  
 wind speed (Section 2.1) and also to the surface temperature monitored by infrared sensing. Note that the  
 520 different temperature measurements are not intercalibrated and may present a limited bias of 1°C. Table 2  
 summarizes the average, minimum and maximum values for 3m temperature, surface temperature, humidity  
 and isotopic composition.



525 **Figure 8:** hourly average  $\delta D$  (‰) in dark blue, hourly average  $\delta^{18}O$  (‰) in green,  $d$ -excess (‰) smoothed on  
 a 3 hours span in light blue, and hourly average of the specific humidity (ppmv) in red measured by the  
 Picarro during the campaign; comparison with 3m temperature (purple, °C), difference between ground and  
 3m temperature (purple shade, °C), wind direction (grey dots, °) and speed (black line).

530 **Table 2:** Average, minimum and maximum values over the whole campaign for air temperature ( $T_{3m}$ ), snow  
 surface temperature ( $T_{surf}$ ), specific humidity ( $q$ ),  $\delta D$  (‰),  $\delta^{18}O$  (‰), and 3 hour smoothed  $d$ -excess (‰).

	Average	Minimum	Maximum
$T_{3m}$ (°C)	-31.2	-42.6	-24.6
$T_{surf}$ (°C)	-31.5	-46.1	-21.2
$q$ (ppmv)	589	161	977
$\delta D$ (‰)	-491	-558	-393
$\delta^{18}O$ (‰)	-68.2	-77.1	-53.9
$d$ -ex (‰)	55.1	21	88

540 Even though the sun is never actually passing below the horizon, when the zenithal angle is low, snow  
 surface radiation deficit generates a strong radiative cooling of the surface which leads to stratification of the  
 atmospheric boundary layer. Daily cycles are clearly visible in all the variables. Greater diurnal temperature  
 variations are observed at the surface than at 3 meters even though average temperatures remain similar as  
 already observed in Kohnen (van As et al., 2006). Day temperature at the surface rises up to 8°C higher than  
 at 3 meters during the period from December 26<sup>th</sup> 2014 to January 4<sup>th</sup> 2015. After January the 4<sup>th</sup>, differences  
 545 remain small (less than 2°C). This first difference will lead us to distinguish the two regimes to further  
 investigate: a first one from December 26<sup>th</sup> 2014 to January 4<sup>th</sup> 2015, and a second one from January the 5<sup>th</sup>  
 to January the 17<sup>th</sup> 2015.

550 Table 3 compares the average values, the diurnal amplitudes and the trends within the different datasets.  
 Temperature is higher during Regime 1, probably due to the proximity to the solar solstice. Diurnal  
 amplitudes in air temperature and humidity are significantly higher in regime 2 than in regime 1. In regime 1,



isotopic daily cycles are dumped and completely erased from the 1<sup>st</sup> of January to the 3<sup>rd</sup> of January, whereas daily cycles are important for regime 2 (in phase with those of temperature); a significant day to day trend appears during the regime 1 with almost -1‰/day for  $\delta^{18}\text{O}$  and is not present in the regime 2 (0.07‰/day for  $\delta^{18}\text{O}$ ).

555

*Table 3: Average, daily amplitude and daily trend over the whole campaign for air temperature ( $T_{3m}$ , °C), snow surface temperature ( $T_{surf}$ , °C), specific humidity ( $q$ , ppmv),  $\delta D$  (‰),  $\delta^{18}\text{O}$  (‰), and smoothed  $d$ -excess (‰).*

560

	Regime 1 : from 26/12 to 04/01			Regime 2 : from 05/01 to 17/01		
	Average	Amplitude	Trend (/day)	Average	Amplitude	Trend (/day)
$T_{3m}$ (°C)	-29.9	$7.6 \pm 0.2$	$-0.29 \pm 0.02$	-32.4	$11.9 \pm 0.2$	$-0.38 \pm 0.02$
$T_{surf}$ (°C)	-30.2	$14.2 \pm 0.4$	$-0.34 \pm 0.05$	-32.6	$16.2 \pm 0.3$	$-0.47 \pm 0.03$
$q$ (ppmv)	631	$341 \pm 20$	$-24 \pm 3$	541	$521 \pm 13$	$-39 \pm 2$
$\delta D$ (‰)	-490	$14 \pm 3$	$-3.7 \pm 0.4$	-495	$38 \pm 2$	$-0.8 \pm 0.3$
$\delta^{18}\text{O}$ (‰)	-68.1	$1.4 \pm 0.6$	$-0.92 \pm 0.06$	-68.9	$5.4 \pm 0.4$	$-0.07 \pm 0.04$
$d$ -ex (‰)	54.9	$8 \pm 1$	$3.7 \pm 0.2$	56.2	$13 \pm 2$	$-0.2 \pm 0.2$

We attribute the difference between the two regimes to changes in atmospheric stability, in particular during the "night". Indeed, during day time, the convection enables strong mixing in both regime 1 and regime 2. However, significant differences are noticeable in the nocturnal stability between regime 1 and 2 which impact the night-time turbulent mixing.

565

Atmospheric static stability is further assessed using the Richardson number (Richardson, 1920), which is a ratio between the square of the Brunt-Väisälä frequency ( $N = \sqrt{\frac{g}{\theta} \frac{d\theta}{dz}}$  where  $\theta = T(P_0/P)^{R/c_p}$  is the potential temperature calculated from  $P_0$  the standard reference pressure,  $R$  the gas constant of air and  $c_p$  the specific heat capacity) and the square of the horizontal wind gradient (see supplementary material part 2). During regime 1, the Richardson number experiences important daily cycles, rising higher than 0.2 during night time, indicating a stable and well stratified boundary layer and dropping lower than 0 during daytime indicating a non-stable, convective atmosphere (King et al., 2006). The Richardson number is in particular really large for the nights from 1<sup>st</sup> of January to the 3<sup>rd</sup> of January (rising up to 0.85) highlighting an enhanced nighttime stratification during this period. The regime 1 is so characterized by a well-marked diurnal cycle with a convective activity during the "day" and a well stably stratified atmospheric boundary layer during the "night". By contrast, the Richardson number is lower during the night in regime 2 which leads to smaller diurnal cycles of stratification. This can be explained by stronger winds during the nights in regime 2 (figure 9) which enhance the turbulent mixing in the atmospheric boundary layer and tends to reduce the stratification.

570

575

580

We now investigate the mean daily cycle of all data during each regime. For this purpose, the trend is removed by subtracting to all data the average value of the day. We then produce a mean value for each hour of the day over the whole regime. The correlations between the average daily cycles of isotopic composition, 3m temperature, 3m wind speed and surface temperature are given on Table 4. 3m temperature is less strongly correlated with surface temperature during regime 1 compared to regime 2. During regime 2 nighttime, the atmosphere is more turbulent and therefore atmospheric mixing is more efficient. For a more stratified nocturnal atmosphere (regime 1), we expect surface temperature to be less correlated to 3m temperature and also to isotopic composition.

585

590



595

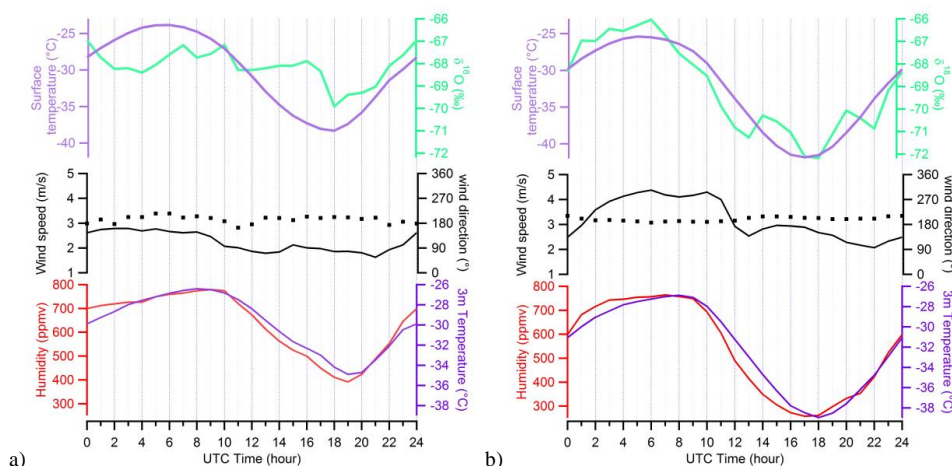
*Table 4: Slope and correlation coefficient between the different data average daily cycle: for each data, the average of the day was removed and a trend-free daily cycle for each regime was produced*

	Regime 1: from 26/12 to 04/01		Regime 2: from 05/01 to 17/01	
	Slope	r <sup>2</sup>	Slope	r <sup>2</sup>
$\delta D$ (‰) vs $q$ (ppmv)	$0.043 \pm 0.005$	0.79	$0.071 \pm 0.003$	0.96
$\delta D$ (‰) vs $T_{3m}$ (°C)	$2.0 \pm 0.2$	0.74	$3.2 \pm 0.2$	0.94
$\delta D$ (‰) vs $T_{surf}$ (°C)	$0.95 \pm 0.2$	0.58	$2.3 \pm 0.1$	0.95
$\delta D$ (‰) vs $\delta^{18}O$ (‰)	$6.0 \pm 1.3$	0.48	$6.5 \pm 0.6$	0.85
$q$ (ppmv) vs $T_{3m}$ (°C)	$45 \pm 2$	0.94	$44 \pm 2$	0.96
$q$ (ppmv) vs $T_{surf}$ (°C)	$24 \pm 2$	0.89	$32 \pm 1$	0.98
$T_{3m}$ (°C) vs $T_{surf}$ (°C)	$0.49 \pm 0.05$	0.80	$0.69 \pm 0.04$	0.92

600 We also observe that the correlation of surface isotopic composition and temperature, and between  $\delta^{18}O$  and  $\delta D$  is stronger for regime 2 (turbulent nocturnal atmosphere) than for regime 1 (stratified nocturnal atmosphere). An explanation for this correlation could be the temperature influence on the fractionation at the snow-air interface. In the case of regime 2, as the turbulence allows efficient air mass mixing, the isotopic composition at 2 meters is directly related to what is happening at the surface; hence the isotopic composition is strongly correlated with surface temperature. Such a situation was already described in NEEM station in Greenland (Steen-Larsen et al., 2013), where similar temperature and water vapour isotopic composition cycles were observed during 10 days, leading to the conclusion that the snow surface was acting successively as a sink during the night and as a source during the day. They also emitted the hypothesis that the vapour isotopic composition could be at equilibrium with the snow one, at least during part of the day. Exchange with the vapour could also have strong impact on snow metamorphism in Concordia, as observed in NEEM (Steen-Larsen et al., 2014a).

615 In the case of regime 1, when atmosphere is at least part of the time stratified, the mixing of the first layers of the atmosphere is not efficiently done by turbulence. In these situations happening mostly at night, the ground is cooling faster than the air above it, creating vertical gradients in moisture content of the atmosphere (van As and van den Broeke, 2006).

620 We now investigate the timing of the average diurnal cycles (Figure 9). By comparing the position of the slope at the mid height, we notice a shift of approximately 2 hours between surface and 3m temperature. Specific humidity average daily cycle is synchronised with 3m temperature in both regimes 1 and 2. For regime 1, no diurnal cycle appears in surface vapour isotopic composition. For regime 2, the daily cycle of surface vapour isotopic composition is synchronised with surface temperature, and therefore shifted 2 hours earlier than 3m temperature and humidity. This is consistent with the hypothesis of temperature-driven exchanges of molecules between the air and the snow surface in regime 2. This hypothesis will be discussed in more details in part 3.3.



630 **Figure 9:** Comparison of average daily cycles (UTC time) of 3m temperature (light purple, °C), surface temperature (dark purple), specific humidity (red, ppmv), wind speed (black line, m/s), wind direction (black dots, °),  $\delta^{18}\text{O}$  (green, ‰) for a) regime 1 and b) regime 2.

The diurnal amplitude that we measured (38‰ for  $\delta\text{D}$  in average during the regime 2) is within the range obtained in previous studies in Greenland. In NEEM, daily cycles up to 36‰ for  $\delta\text{D}$  were measured during summer campaigns (Steen-Larsen et al., 2013), much more important than the one on the coastal areas of Greenland with peak to peak amplitudes of variations of 1‰ for  $\delta^{18}\text{O}$  in Ivittuut, Greenland (Bonne et al., 2014). Similar pattern is observed around Antarctica, near coastal areas, on a ship near Syowa station, isotopic composition variations are dominated by day to day evolution and there are no diurnal cycles (Kurita et al., under review).

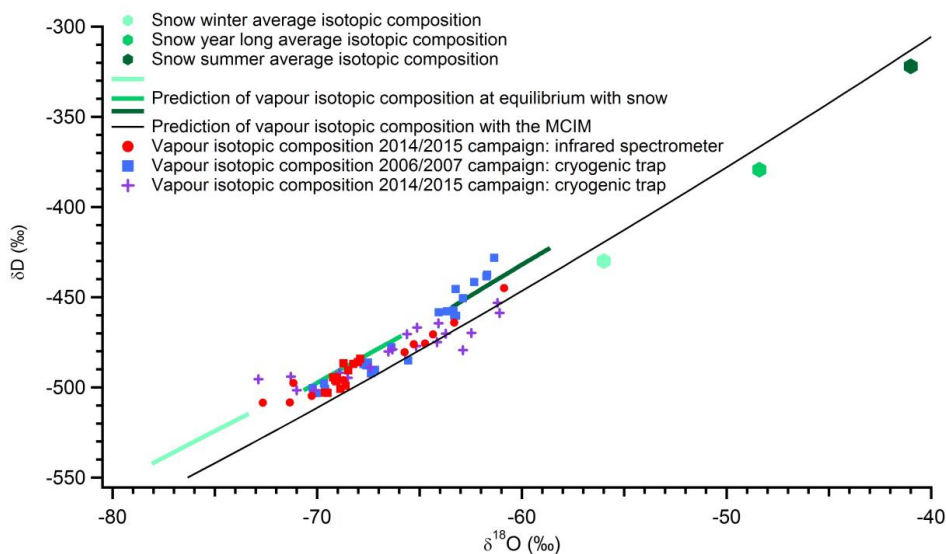
### 640 3.3. Local water vapour $\delta\text{D}$ - $\delta^{18}\text{O}$ relationship and snow surface interactions

Figure 10 presents the  $\delta\text{D}$  and  $\delta^{18}\text{O}$  isotopic composition during the 2014/2015 campaign, for continuous measurements, cold trap data, together with earlier cold trap data from 2006/2007. We observe that all these data depict a common range of isotopic composition and align on a similar slope.

We observe very low (around 5)  $\delta\text{D}$  and  $\delta^{18}\text{O}$  slopes measured using infrared spectroscopy on site and post campaign mass spectrometry of the cryogenic trapping samples (table 5). In fact, publication of the 2006/2007 cold trap data had been postponed until an explanation for such low vapour line was identified, by fear of sampling vapour from the station generator. As stated in section 2.5, no such contamination occurred. This slope is much lower than observed in Greenland (Bonne et al., 2014; Steen-Larsen et al., 2013). A very low slope for  $\delta\text{D}$  vs  $\delta^{18}\text{O}$  in water vapour is not unexpected as Dome C is very far on the distillation path and air masses are very depleted in heavy isotopologues (Touzeau et al., 2015). Indeed, for a Rayleigh distillation, the local relative variations of the isotopic composition of  $\delta\text{D}$  and  $\delta^{18}\text{O}$  are defined by:

$$\frac{d\delta\text{D}}{d\delta^{18}\text{O}} = \frac{\alpha_{\text{D}} - 1}{\alpha_{18} - 1} \frac{1 + \delta\text{D}}{1 + \delta^{18}\text{O}} \quad (2)$$

where  $\alpha_{\text{D}}$  and  $\alpha_{18}$  are respectively the equilibrium fractionation coefficients of HDO and  $\text{H}_2^{18}\text{O}$  (Jouzel and Merlivat, 1984). In the average condition of the campaign ( $T = -31.5^\circ\text{C}$  and isotopic composition from table 2), even if  $(\alpha_{\text{D}} - 1)/(\alpha_{18} - 1) = 9.71$ , the very low value of  $\delta\text{D}$  (around -500‰) brings down the slope  $\delta\text{D}$  and  $\delta^{18}\text{O}$  to 5.3‰/‰. Note that the important d-excess values obtained in section 3.2. are due to the very low slope between  $\delta\text{D}$  and  $\delta^{18}\text{O}$ , and not necessarily to important kinetic effects in this case.



665 *Figure 10:  $\delta D$  and  $\delta^{18}O$  plots: red is the daily average isotopic composition from the Picarro (circles :  
regime 1, squares regime 2), purple crosses are the cold trap isotopic composition from 2014/2015  
670 campaign, blue squares are the cold trap isotopic composition from 2006/2007, green hexagons are the  
isotopic composition of the snow (Touzeau et al., 2015) (light is the average composition minus 1 standard  
deviation, mid is the average composition and dark is the average composition plus 1 standard deviation),  
675 green lines are the respecting calculated equilibrium fractionation in the range of temperature observed  
during the campaign (Majoube, 1971) (local origin thereafter) and black line is the curve established with a  
Rayleigh distillation in the MCIM (remote origin thereafter)*

We now discuss in details the possible drivers of the isotopic composition of water vapour at Dome C  
675 following several hypotheses: 1-local origin (equilibrium between surface snow and water vapour); 2- remote  
origin (distillation of a water mass from the coast).

For the first hypothesis, we used the range of annual isotopic composition of the snow at Dome C (Touzeau  
680 et al., 2015), represented by green hexagons (average value plus and minus one standard deviation). The  
slope between  $\delta D$  and  $\delta^{18}O$  of the snow annual isotopic composition is 7.2‰/‰, already lower than 8. From  
these values, we calculate the corresponding vapour isotopic composition in the range of summer  
temperature (-20 to -45°C) using standard equilibrium fractionation coefficients (Majoube, 1971; Merlivat  
and Nief, 1967). The range of calculated vapour isotopic contents is consistent with observed vapour: from  
685 the average value of snow  $\delta^{18}O = -48.4\text{‰}$ , we get a vapour predicted  $\delta^{18}O = -68.2\text{‰}$  at -35°C which lies  
within the values measured by the Picarro (on average over the campaign  $\delta^{18}O = -68.9\text{‰}$ ). The slope between  
 $\delta D$  and  $\delta^{18}O$  on the other hand is higher than the one observed: 6.5‰/‰ vs 5.3‰/‰ for the Picarro and even  
4.8‰/‰ for the cold traps. The same calculation with the equilibrium fractionation coefficients from Ellehøj  
et al. (2013) can predict relevant  $\delta^{18}O$  and  $\delta D$  values and more realistic slopes (5.7‰/‰).

690



695 *Table 5: Slope and correlation coefficients between the different datasets. Picarro and meteorological data are daily average data. Equilibrium fractionation slopes are calculated from the average values (average, plus and minus one standard deviation) with Majoube fractionation coefficients (high M, med M, low M) or Ellehøj fractionation coefficients (med E)*

		Data for all season	
		Slope	r <sup>2</sup>
Picarro data	δD (‰) vs q (ppmv)	0.12 ± 0.02	0.61
	δD (‰) vs T <sub>3m</sub> (°C)	3.7 ± 1.5	0.22
	δD (‰) vs T <sub>surf</sub> (°C)	4.3 ± 1.2	0.30
	δD (‰) vs δ <sup>18</sup> O (‰)	5.3 ± 0.3	0.92
	q (ppmv) vs T <sub>3m</sub> (°C)	43 ± 6	0.69
	q (ppmv) vs T <sub>surf</sub> (°C)	45 ± 5	0.79
Meteo data	T <sub>3m</sub> (°C) vs T <sub>surf</sub> (°C)	0.7 ± 0.1	0.63
Trapping 2006/07	δD (‰) vs δ <sup>18</sup> O (‰)	4.6 ± 0.7	0.82
Trapping 2014/15	δD (‰) vs δ <sup>18</sup> O (‰)	4.8 ± 0.4	0.90
Equilibrium fractionation	δD (‰) vs δ <sup>18</sup> O (‰) high M	7.02	Th.
	δD (‰) vs δ <sup>18</sup> O (‰) med M	6.50	Th.
	δD (‰) vs δ <sup>18</sup> O (‰) low M	5.99	Th.
	δD (‰) vs δ <sup>18</sup> O (‰) med E	5.65	Th.
MCIM	δD (‰) vs δ <sup>18</sup> O (‰) at -35°C	6.11	Th.

700

We now analyse the effect of the distillation on the isotopic composition of the water vapour. For this test, we used Mixed Cloud Isotopic Model (MCIM) to compute the isotopic composition of the vapour. The MCIM is a Rayleigh model taking into account microphysical properties of clouds and in particular accounting for mixed phases (Ciais and Jouzel, 1994). The model was tuned with snow isotopic composition of an Antarctic transect from Terra Nova Bay to Dome C to accurately reproduce the isotopic composition of the Antarctic Plateau (Winkler et al., 2012). For instance, the model predicts an average value of snow isotopic composition at Dome C of -51‰ for an average site temperature of -54.5°C when the measurements indicated -50.7‰; note that the model take into account an inversion temperature and that the condensation temperature  $T_{cond}$  is deduced from the surface temperature  $T_{surf}$  through (Ekaykin and Lipenkov, 2009):

710

$$T_{cond} = 0.67 \times T_{surf} - 1.2 \quad (3)$$

The prediction of average vapour isotopic composition by the MCIM is  $\delta^{18}\text{O} = -51.6\text{‰}$  at  $-35\text{°C}$  which is much higher than the average vapour measurements ( $\delta^{18}\text{O} = -68.9\text{‰}$ ). However, the MCIM manages to predict the isotopic composition of the summer precipitation ( $\delta^{18}\text{O} = -37\text{‰}$  at  $-35\text{°C}$  for the model compared to values rising up to  $-39\text{‰}$  for matching temperature in Dome C summer precipitation. Therefore, we conclude that the vapour isotopic composition seems to be principally influenced by local effects. Note that the slope between  $\delta\text{D}$  and  $\delta^{18}\text{O}$  predicted by the MCIM is around  $6.1\text{‰/‰}$  which is also higher than the one observed during the campaign (between 4.6 and 5.3 for the different datasets).

720

The precipitation amount in Dome C is less than 10 cm per year (Genthon et al., 2015). Each precipitation event does not form a complete layer of snow and is mixed with earlier snowfall possibly deposited under the earlier winter conditions. The snow isotopic composition is therefore a mix new snowfall and older snow. This phenomenon is amplified by drift and blowing snow (Libois et al., 2014). A mixing between a large range of source isotopic compositions should be considered to compute the local origin hypotheses which could explain the bias of the slope predicted by equilibrium from a single snow composition compared with experimental data.

725

730



#### 4. Conclusion

735 In this study, we assessed the relevance of infrared spectrometry to measure isotopic composition of water at concentration as low as the ones encountered over the Antarctic Plateau. Apart from the logistic challenges involved in the installation of spectrometers in remote areas; humidity levels, very depleted samples and important local variability imply a technical challenge that the new infrared spectroscopy techniques overcame.

740 Allan variance measurements in the laboratory indicated the possibility to use Picarro and HiFI spectrometers at humidity as low as 200 ppmv and with almost no loss of precision from 500 ppmv (limit of precision of 0.1‰  $\delta^{18}\text{O}$  and for 1.1‰ for  $\delta\text{D}$ ). Identical measurements in the field showed it was possible to reach similar results in the field even though great care in the environment where the instruments are deployed should be addressed.

745 For such humidities, the linearity of the instruments is not guaranteed toward humidity and regular calibrations on the field are necessary. In this particular study, it was not possible to calibrate regularly the instruments in the field for logistical reasons, so we bracketed the drift of the instrument by series of calibration in the lab. This is not the optimal method and results in important error bars compared to the performances of the instrument. The uncertainty of the isotopic composition measurement is therefore 6‰ for  $\delta\text{D}$  and 0.7‰ for  $\delta^{18}\text{O}$ . We have further validated these measurements through i) a comparison of the data acquired by infrared spectrometry with cryogenic trapping samples, ii) a protocol to calibrate on the SMOW-SLAP scale at  $\delta^{18}\text{O}$  lower than the SLAP  $\delta^{18}\text{O}$  value (-55.5‰). This calibration demonstrated that our Picarro instrument is linear in  $\delta^{18}\text{O}$  down to -80‰ in  $\delta^{18}\text{O}$  and stays almost linear down to -110‰. This is essential for our study since the mean  $\delta^{18}\text{O}$  value was -68.2‰ at Concordia between December the 25<sup>th</sup> 2014 and January the 17<sup>th</sup> 2015.

760 Two different regimes have been identified during the campaign: a first one from December the 26<sup>th</sup> 2014 to January the 4<sup>th</sup> 2015 and a second from January the 5<sup>th</sup> to January the 17<sup>th</sup> 2015. The main difference between the two regimes on isotopic composition is the amplitude of the daily cycles: large and regular during regime 2 and small and irregular in regime 1 and even an almost erased one from January the 1<sup>st</sup> to January the 4<sup>th</sup> 2015. For regime 1, correlation of humidity with surface temperature is lowered and isotopic composition is almost stable whereas for regime 2, there is an almost perfect correlation for both humidity and isotopic composition with temperature. We attribute these differences to difference in the stability of the atmosphere. 765 For regime 1, we explain the drop of correlation by a weakly turbulent boundary layer during which temperature, humidity and isotopic composition diurnal cycles are truncated compared to a second one characterised by efficient turbulence with important diurnal cycles and almost perfect correlation between the snow surface temperature and the first meters of the atmosphere. The second regime therefore appears to be characterised by equilibrium between the isotopic composition of vapour over the first meters and the one of the snow as already shown for Greenland (Steen-Larsen et al., 2013). 770

Temperature cycles seem to be directly responsible for isotopic composition cycles, at least in Regime 2, through equilibrium fractionation in sublimation/condensation cycles. At first order, it seems the snow isotopic composition is therefore influencing directly the vapour through fractionation at phase change. The vapour isotopic composition average value matches the one obtained by equilibrium fractionation of the local snow. Still the measured slope between  $\delta\text{D}$  and  $\delta^{18}\text{O}$  cannot be explained purely by equilibrium fractionation from local snow. We cannot rule out a contribution of horizontal air advection from inland locations, transported by southward winds and providing small amounts of very depleted moisture. 775

780 Finally, our study opens new perspectives in the influence of post deposition effects and their importance for the water stable isotope signal recorded in deep ice cores. In particular, we have shown that the relationship between water vapour  $\delta^{18}\text{O}$  and temperature can be erased by weakly turbulent regimes. Yearlong monitoring of the isotopic composition of the water vapour could help identify how often these conditions happen, and



785 also if the snow isotopic composition could present biased relationship toward seasonality, temperature or  
precipitation.

790 **Acknowledgments:** The research leading to these results has received funding from the European Research  
Council under the European Union's Seventh Framework Programme (FP7/2007-2013) / ERC grant  
agreement n° [306045]. We acknowledge the programs NIVO and GLACIO and all the IPEV that made this  
campaign possible, LGGE and LIPHY for providing logistic advice and support. We thank Catherine Ritz,  
Anais Orsi and Xavier Fain for their help during the preparation of the mission. Many thanks to Philippe  
Ricaud, Doris Thuillier, Nicolas Caillon, Bruno Jourdain, Olivier Magand and all the eleventh winter-over  
795 team for your support and your presence in Concordia. Thanks to Hubert Gallée for all the discussions about  
polar meteorology.



## 800 Bibliography

- Aemisegger, F., Sturm, P., Graf, P., Sodemann, H., Pfahl, S., Knohl, A. and Wernli, H. (2012) Measuring variations of  $\delta^{18}\text{O}$  and  $\delta^2\text{H}$  in atmospheric water vapour using two commercial laser-based spectrometers: an instrument characterisation study. *Atmos. Meas. Tech.* 5, 1491-1511.
- 805 Bailey, A., Noone, D., Berkelhammer, M., Steen-Larsen, H.C. and Sato, P. (2015) The stability and calibration of water vapor isotope ratio measurements during long-term deployments. *Atmos. Meas. Tech. Discuss.* 8, 5425-5466.
- Bonne, J.-L., Steen-Larsen, H.C., Risi, C., Werner, M., Sodemann, H., Lacour, J.-L., Fettweis, X., Cesana, G., Delmotte, M., Cattani, O., Vallelonga, P., Kjær, H.A., Clerbaux, C., Sveinbjörnsdóttir, Á.E. and Masson-Delmotte, V. (2015) The summer 2012 Greenland heat wave: in situ and remote sensing observations of water vapour isotopic composition during an atmospheric river event. *Journal of Geophysical Research: Atmospheres*, 2014JD022602.
- 815 Bonne, J.L., Masson-Delmotte, V., Cattani, O., Delmotte, M., Risi, C., Sodemann, H. and Steen-Larsen, H.C. (2014) The isotopic composition of water vapour and precipitation in Ivittuut, southern Greenland. *Atmos. Chem. Phys.* 14, 4419-4439.
- Cappa, C.D., Hendricks, M.B., DePaolo, D.J. and Cohen, R.C. (2003) Isotopic fractionation of water during evaporation. *J. Geophys. Res.-Atmos.* 108, 10.
- 820 Charles, C.D., Rind, D., Jouzel, J., Koster, R.D. and Fairbanks, R.G. (1994) Glacial-Interglacial Changes in Moisture Sources for Greenland: Influences on the Ice Core Record of Climate. *Science* 263, 508-511.
- Ciais, P. and Jouzel, J. (1994) Deuterium and oxygen 18 in precipitation: Isotopic model, including mixed cloud processes. *Journal of Geophysical Research: Atmospheres* 99, 16793-16803.
- 825 Craig, H., Gordon, A. (1965) Deuterium and oxygen 18 variations in the ocean and the marine atmosphere. *Stable Isotopes in Oceanic Studies and Paleotemperatures*, 130.
- Crosson, E.R. (2008) A cavity ring-down analyzer for measuring atmospheric levels of methane, carbon dioxide, and water vapor. *Appl. Phys. B* 92, 403-408.
- 830 Dansgaard, W. (1964) Stable isotopes in precipitation. *Tellus* 16, 436-468.
- Ekaykin, A.A. and Lipenkov, V.Y. (2009) Formation of the ice core isotopic composition. *低温科学 = Low Temperature Science* 68, 299-314.
- Ekaykin, A.A., Lipenkov, V.Y., Barkov, N.I., Petit, J.R. and Masson-Delmotte, V. (2002) Spatial and temporal variability in isotope composition of recent snow in the vicinity of Vostok station, Antarctica: implications for ice-core record interpretation. *Annals of Glaciology* 35, 181-186.
- 835 Ekaykin, A.A., Lipenkov, V.Y., Kuzmina, I.N., Petit, J.R., Masson-Delmotte, V. and Johnsen, S.J. (2004) The changes in isotope composition and accumulation of snow at Vostok station, East Antarctica, over the past 200 years. *Annals of Glaciology* 39, 569-575.
- 840 Ellehøj, M.D., Steen-Larsen, H.C., Johnsen, S.J. and Madsen, M.B. (2013) Ice-vapor equilibrium fractionation factor of hydrogen and oxygen isotopes: Experimental investigations and implications for stable water isotope studies. *Rapid Communications in Mass Spectrometry* 27, 2149-2158.
- 845 EPICA (2004) Eight glacial cycles from an Antarctic ice core. *Nature* 429, 623-628.
- Fawcett, P.J., Ágústsdóttir, A.M., Alley, R.B. and Shuman, C.A. (1997) The Younger Dryas Termination and North Atlantic Deep Water Formation: Insights from climate model simulations and Greenland Ice Cores. *Paleoceanography* 12, 23-38.
- 850 Frezzotti, M., Gandolfi, S., La Marca, F. and Urbini, S. (2002) Snow dunes and glazed surfaces in Antarctica: new field and remote-sensing data. *Annals of Glaciology* 34, 81-88.
- Genthon, C., Six, D., Favier, V., Lazzara, M. and Keller, L. (2011) Atmospheric Temperature Measurement Biases on the Antarctic Plateau. *J. Atmos. Ocean. Technol.* 28, 1598-1605.
- 855 Genthon, C., Six, D., Gallée, H., Grigioni, P. and Pellegrini, A. (2013) Two years of atmospheric boundary layer observations on a 45-m tower at Dome C on the Antarctic plateau. *Journal of Geophysical Research: Atmospheres* 118, 3218-3232.



- 860 Genthon, C., Six, D., Scarchilli, C., Ciardini, V. and Frezzotti, M. (2015) Meteorological and snow accumulation gradients across Dome C, East Antarctic plateau. *International Journal of Climatology*, n/a-n/a.
- Genthon, C., Town, M.S., Six, D., Favier, V., Argentini, S. and Pellegrini, A. (2010) Meteorological atmospheric boundary layer measurements and ECMWF analyses during summer at Dome C, Antarctica. *J. Geophys. Res.-Atmos.* 115, 12.
- 865 Gorski, G., Strong, C., Good, S.P., Bares, R., Ehleringer, J.R. and Bowen, G.J. (2015) Vapor hydrogen and oxygen isotopes reflect water of combustion in the urban atmosphere. *Proceedings of the National Academy of Sciences* 112, 3247-3252.
- Helliker, B.R., Roden, J.S., Cook, C. and Ehleringer, J.R. (2002) A rapid and precise method for sampling and determining the oxygen isotope ratio of atmospheric water vapor. *Rapid Communications in Mass Spectrometry* 16, 929-932.
- 870 Hoshina, Y., Fujita, K., Nakazawa, F., Iizuka, Y., Miyake, T., Hirabayashi, M., Kuramoto, T., Fujita, S. and Motoyama, H. (2014) Effect of accumulation rate on water stable isotopes of near-surface snow in inland Antarctica. *Journal of Geophysical Research: Atmospheres* 119, 274-283.
- IAEA (2009) Reference Sheet for VSMOW2 and SLAP2 international measurement standards. International Atomic Energy Agency, Vienna.
- 875 Johnsen, S.J., Clausen, H.B., Cuffey, K.M., Hoffmann, G. and Creyts, T.T. (2000) Diffusion of stable isotopes in polar firn and ice: the isotope effect in firn diffusion. *Physics of ice core records*, 121-140.
- Jouzel, J., Alley, R., Cuffey, K., Dansgaard, W., Grootes, P., Hoffmann, G., Johnsen, S., 880 Koster, R., Peel, D. and Shuman, C. (1997) Validity of the temperature reconstruction from water isotopes in ice cores. *JOURNAL OF GEOPHYSICAL RESEARCH-ALL SERIES-102*, 26,471-426,487.
- Jouzel, J., Delaygue, G., Landais, A., Masson-Delmotte, V., Risi, C. and Vimeux, F. (2013) 885 Water isotopes as tools to document oceanic sources of precipitation. *Water Resources Research* 49, 7469-7486.
- Jouzel, J. and Merlivat, L. (1984) Deuterium and oxygen 18 in precipitation: Modeling of the isotopic effects during snow formation. *Journal of Geophysical Research: Atmospheres* 89, 11749-11757.
- 890 King, J.C., Argentini, S.A. and Anderson, P.S. (2006) Contrasts between the summertime surface energy balance and boundary layer structure at Dome C and Halley stations, Antarctica. *Journal of Geophysical Research: Atmospheres* 111, n/a-n/a.
- Krinner, G., Genthon, C. and Jouzel, J. (1997) GCM analysis of local influences on ice core  $\delta$  signals. *Geophysical Research Letters* 24, 2825-2828.
- 895 Landais, A., Barkan, E. and Luz, B. (2008) Record of  $\delta^{18}O$  and  $17O$ -excess in ice from Vostok Antarctica during the last 150,000 years. *Geophysical Research Letters* 35, L02709.
- Landsberg, J. (2014) Development of an OF-CEAS laser spectrometer for water vapor isotope measurements at low water concentrations. University of Groningen.
- 900 Landsberg, J., Romanini, D. and Kerstel, E. (2014) Very high finesse optical-feedback cavity-enhanced absorption spectrometer for low concentration water vapor isotope analyses. *Opt. Lett.* 39, 1795-1798.
- LeGrande, A.N. and Schmidt, G.A. (2006) Global gridded data set of the oxygen isotopic composition in seawater. *Geophysical Research Letters* 33, n/a-n/a.
- 905 Libois, Q., Picard, G., Arnaud, L., Morin, S. and Brun, E. (2014) Modeling the impact of snow drift on the decameter-scale variability of snow properties on the Antarctic Plateau. *Journal of Geophysical Research: Atmospheres* 119, 662-611,681.
- Lorius, C., Merlivat, L. and Hagemann, R. (1969) Variation in the mean deuterium content of precipitations in Antarctica. *Journal of Geophysical Research* 74, 7027-7031.
- 910 Luz, B., Barkan, E., Yam, R. and Shemesh, A. (2009) Fractionation of oxygen and hydrogen isotopes in evaporating water. *Geochimica et Cosmochimica Acta* 73, 6697-6703.
- Majoube, M. (1971) FRACTIONATION IN O-18 BETWEEN ICE AND WATER VAPOR. *J. Chim. Phys.-Chim. Biol.* 68, 625-&.
- 915 Masson-Delmotte, V., Buiron, D., Ekaykin, A., Frezzotti, M., Gallée, H., Jouzel, J., Krinner, G., Landais, A., Motoyama, H., Oerter, H., Pol, K., Pollard, D., Ritz, C., Schlosser, E., Sime, L.C., Sodemann, H., Stenni, B., Uemura, R. and Vimeux, F. (2011) A



- comparison of the present and last interglacial periods in six Antarctic ice cores. *Clim. Past* 7, 397-423.
- 920 Masson-Delmotte, V., Hou, S., Ekaykin, A., Jouzel, J., Aristarain, A., Bernardo, R.T., Bromwich, D., Cattani, O., Delmotte, M., Falourd, S., Frezzotti, M., Gallée, H., Genoni, L., Isaksson, E., Landais, A., Helsen, M.M., Hoffmann, G., Lopez, J., Morgan, V., Motoyama, H., Noone, D., Oerter, H., Petit, J.R., Royer, A., Uemura, R., Schmidt, G.A., Schlosser, E., Simões, J.C., Steig, E.J., Stenni, B., Stievenard, M., van den Broeke, M.R., van de Wal, R.S.W., van de Berg, W.J., Vimeux, F. and White, J.W.C. (2008) A Review of
- 925 Antarctic Surface Snow Isotopic Composition: Observations, Atmospheric Circulation, and Isotopic Modeling\*. *J. Clim.* 21, 3359-3387.
- Merlivat, L. (1978) MOLECULAR DIFFUSIVITIES OF (H<sub>2</sub>O)-O-16 AND (H<sub>2</sub>O)-O-18 IN GASES. *J. Chem. Phys.* 69, 2864-2871.
- 930 Merlivat, L. and Nief, G. (1967) Fractionnement isotopique lors des changements d'état solide-vapeur et liquide-vapeur de l'eau à des températures inférieures à 0°C. *Tellus* 19, 122-127.
- Neumann, T.A. and Waddington, E.D. (2004) Effects of firn ventilation on isotopic exchange. *Journal of Glaciology* 50, 183-194.
- 935 Petit, J.R., Jouzel, J., Pourchet, M. and Merlivat, L. (1982) A detailed study of snow accumulation and stable isotope content in Dome C (Antarctica). *Journal of Geophysical Research: Oceans* 87, 4301-4308.
- Ricaud, P., Genthon, C., Durand, P., Attié, J.L., Carminati, F., Canut, G., Vanacker, J.F., Moggio, L., Courcoux, Y., Pellegrini, A. and Rose, T. (2012) Summer to Winter Diurnal Variabilities of Temperature and Water Vapour in the Lowermost Troposphere as
- 940 Observed by HAMSTRAD over Dome C, Antarctica. *Boundary-Layer Meteorol* 143, 227-259.
- Richardson, L.F. (1920) The Supply of Energy from and to Atmospheric Eddies.
- Risi, C., Bony, S., Vimeux, F. and Jouzel, J. (2010) Water-stable isotopes in the LMDZ4 general circulation model: Model evaluation for present-day and past climates and
- 945 applications to climatic interpretations of tropical isotopic records. *Journal of Geophysical Research: Atmospheres* 115, D12118.
- Romanini, D., Ventrillard, I., Méjean, G., Morville, J. and Kerstel, E. (2014) Introduction to Cavity Enhanced Absorption Spectroscopy, in: Gagliardi, G., Loock, H.-P. (Eds.), *Cavity-Enhanced Spectroscopy and Sensing*. Springer Berlin Heidelberg, pp. 1-60.
- 950 Röthlisberger, R., Hutterli, M.A., Sommer, S., Wolff, E.W. and Mulvaney, R. (2000) Factors controlling nitrate in ice cores: Evidence from the Dome C deep ice core. *Journal of Geophysical Research: Atmospheres* 105, 20565-20572.
- Salisbury, J.W., Wald, A. and D'Aria, D.M. (1994) Thermal-infrared remote sensing and Kirchhoff's law: 1. Laboratory measurements. *Journal of Geophysical Research: Solid Earth* 99, 11897-11911.
- 955 Schmidt, G.A., Hoffmann, G., Shindell, D.T. and Hu, Y. (2005) Modeling atmospheric stable water isotopes and the potential for constraining cloud processes and stratosphere-troposphere water exchange. *Journal of Geophysical Research: Atmospheres* 110, D21314.
- 960 Schneebeli, M. and Sokratov, S.A. (2004) Tomography of temperature gradient metamorphism of snow and associated changes in heat conductivity. *Hydrological Processes* 18, 3655-3665.
- Sokratov, S.A. and Golubev, V.N. (2009) Snow isotopic content change by sublimation. *Journal of Glaciology* 55, 823-828.
- 965 Steen-Larsen, H.C., Johnsen, S.J., Masson-Delmotte, V., Stenni, B., Risi, C., Sodemann, H., Balslev-Clausen, D., Blunier, T., Dahl-Jensen, D., Ellehøj, M.D., Falourd, S., Grindsted, A., Gkinis, V., Jouzel, J., Popp, T., Sheldon, S., Simonsen, S.B., Sjolte, J., Steffensen, J.P., Sperlich, P., Sveinbjörnsdóttir, A.E., Vinther, B.M. and White, J.W.C. (2013) Continuous monitoring of summer surface water vapor isotopic composition
- 970 above the Greenland Ice Sheet. *Atmos. Chem. Phys.* 13, 4815-4828.
- Steen-Larsen, H.C., Masson-Delmotte, V., Hirabayashi, M., Winkler, R., Satow, K., Prié, F., Bayou, N., Brun, E., Cuffey, K.M., Dahl-Jensen, D., Dumont, M., Guillevic, M., Kipfstuhl, S., Landais, A., Popp, T., Risi, C., Steffen, K., Stenni, B. and Sveinbjörnsdóttir, A.E. (2014a) What controls the isotopic composition of Greenland surface snow? *Clim. Past* 10, 377-392.
- 975



- 980 Steen-Larsen, H.C., Masson-Delmotte, V., Sjolte, J., Johnsen, S.J., Vinther, B.M., Bréon, F.M., Clausen, H.B., Dahl-Jensen, D., Falourd, S., Fettweis, X., Gallée, H., Jouzel, J., Kageyama, M., Lerche, H., Minster, B., Picard, G., Punge, H.J., Risi, C., Salas, D., Schwander, J., Steffen, K., Sveinbjörnsdóttir, A.E., Svensson, A. and White, J. (2011) Understanding the climatic signal in the water stable isotope records from the NEEM shallow firn/ice cores in northwest Greenland. *Journal of Geophysical Research: Atmospheres* 116, n/a-n/a.
- 985 Steen-Larsen, H.C., Sveinbjörnsdóttir, A.E., Peters, A.J., Masson-Delmotte, V., Guishard, M.P., Hsiao, G., Jouzel, J., Noone, D., Warren, J.K. and White, J.W.C. (2014b) Climatic controls on water vapor deuterium excess in the marine boundary layer of the North Atlantic based on 500 days of in situ, continuous measurements. *Atmos. Chem. Phys.* 14, 7741-7756.
- 990 Touzeau, A., Landais, A., Stenni, B., Uemura, R., Fukui, K., Fujita, S., Guilbaud, S., Ekaykin, A., Casado, M., Barkan, E., Luz, B., Magand, O., Teste, G., Le Meur, E., Baroni, M., Savarino, J., Bourgeois, I. and Risi, C. (2015) Acquisition of isotopic composition for surface snow in East Antarctica and the links to climatic parameters. *The Cryosphere Discuss.* 9, 6275-6313.
- 995 Tremoy, G., Vimeux, F., Cattani, O., Mayaki, S., Souley, I. and Favreau, G. (2011) Measurements of water vapor isotope ratios with wavelength-scanned cavity ring-down spectroscopy technology: new insights and important caveats for deuterium excess measurements in tropical areas in comparison with isotope-ratio mass spectrometry. *Rapid Communications in Mass Spectrometry* 25, 3469-3480.
- 1000 van As, D. and van den Broeke, M.R. (2006) Structure and dynamics of the summertime atmospheric boundary layer over the Antarctic Plateau: 2. Heat, moisture, and momentum budgets. *Journal of Geophysical Research: Atmospheres* 111, n/a-n/a.
- van As, D., van den Broeke, M.R. and Helsen, M.M. (2006) Structure and dynamics of the summertime atmospheric boundary layer over the Antarctic Plateau: 1. Measurements and model validation. *Journal of Geophysical Research: Atmospheres* 111, n/a-n/a.
- 1005 Van Hook, W.A. (1968) Vapor pressures of the isotopic waters and ices. *The Journal of Physical Chemistry* 72, 1234-1244.
- Waddington, E.D., Steig, E.J. and Neumann, T.A. (2002) Using characteristic times to assess whether stable isotopes in polar snow can be reversibly deposited. *Annals of Glaciology* 35, 118-124.
- 1010 Werner, M., Langebroek, P.M., Carlsen, T., Herold, M. and Lohmann, G. (2011) Stable water isotopes in the ECHAM5 general circulation model: Toward high-resolution isotope modeling on a global scale. *Journal of Geophysical Research: Atmospheres* 116, D15109.
- 1015 Winkler, R., Landais, A., Sodemann, H., Dümbgen, L., Prié, F., Masson-Delmotte, V., Stenni, B. and Jouzel, J. (2012) Deglaciation records of  $^{17}\text{O}$ -excess in East Antarctica: reliable reconstruction of oceanic normalized relative humidity from coastal sites. *Clim. Past* 8, 1-16.